

This document is confidential and is proprietary to the American Chemical Society and its authors. Do not copy or disclose without written permission. If you have received this item in error, notify the sender and delete all copies.

Molecular Dynamics Simulations Predict The Pathways via which Pristine Fullerenes Penetrate Bacterial Membranes

Journal:	<i>The Journal of Physical Chemistry</i>
Manuscript ID	jp-2016-06615a.R2
Manuscript Type:	Article
Date Submitted by the Author:	n/a
Complete List of Authors:	Hsu, Pin; University of Southampton, Chemistry Jefferies, Damien; University of Southampton, Chemistry Khalid, Syma; University of Southampton, Chemistry

SCHOLARONE™
Manuscripts

1
2
3 **Molecular Dynamics Simulations Predict The Pathways via which**
4
5 **Pristine Fullerenes Penetrate Bacterial Membranes.**
6
7

8
9 Pin-Chia Hsu,^{a,†} Damien Jefferies^{a,†} and Syma Khalid^{a*}
10
11

12
13
14
15
16
17
18 ^a. School of Chemistry, University of Southampton, Southampton, SO17 1BJ, UK

19 † These authors contributed equally

20
21 * to whom correspondence should be addressed at Email: S.Khalid@soton.ac.uk Tel.:

22
23 +44-2380-594176 Fax: +44-2380-593781
24
25
26
27
28
29
30
31
32
33
34
35
36
37
38
39
40
41
42
43
44
45
46
47
48
49
50
51
52
53
54
55
56
57
58
59
60

Abstract

Carbon fullerenes are emerging as effective devices for different biomedical applications, including the transportation of nanosized drugs and the extraction of harmful oxidants and radicals. It has been proposed that fullerenes could be used as novel antibacterial agents, given the realization that the nanoparticles can kill pathogenic Gram-negative bacteria. To explore this at the molecular level, we simulated C_{60} fullerenes with bacterial membranes using the coarse-grain (CG) molecular dynamics (MD) Martini force field. We find that pristine C_{60} has a limited tendency to penetrate (incomplete core) Re mutant lipopolysaccharide (LPS) leaflets, but the translocation of C_{60} fullerenes into (complete core) Ra mutant LPS leaflets is not thermodynamically favored. Moreover, we show that the permeability of Re LPS bilayers depends sensitively on system temperature, the charge of ambient ions, and the prevalence of POPE defect domains. The different permeabilities are rationalized in terms of transitory head group pore formation, which underpins the translocation of C_{60} into the lipid core. The Re LPS lipids readily form transient micropores when they are linked with monovalent cations, or when they are heated to a high temperature. POPE lipids are shown to be particularly adept at forming these transient surface cavities, and their inclusion into Re LPS membranes facilitates the formation of particularly large pores that are tunneled by C_{60} aggregates of significant size (~ 5 nm wide). After inserting into the lipid core, the aggregates dissociate, and the disbanded nanoparticles migrate to the interface between separate POPE and LPS domains, where they weaken the boundaries between the coexisting lipid fractions and thereby promoting lipid mixing.

Introduction

Since their discovery in 1985,¹ carbon fullerenes have been the subject of intense research due to their interesting chemical properties, and for their potential technological and biomedical applications. For example, their excellent electron acceptor abilities make carbon fullerenes suitable components of novel photovoltaic devices.² Diverse biomedical applications have additionally been proposed for fullerenes, which generally use the ability of these caged compounds to entrap small molecules and thus serve as nanosized gene or drug delivery devices.^{3,4} But more recently, fullerenes have been shown to be bactericidal towards Gram-negative bacteria such as *Escherichia coli* (*E. coli*),^{5,6} suggesting that fullerenes may find future applications in controlling microbial pathogens. C₆₀ nanoparticles seem especially well suited for antibacterial applications compared to metallic nanoparticles or expansive repetitively branched dendrimers, given their small size, which reduces energy barriers to bilayer insertion, and their ability to accommodate diverse surface decoration enabling fine-tuning of particle shape and surface chemistry.^{7,8} As such, work investigating the antibacterial action of fullerenes through the use of experimental techniques has become one of the most topical areas in bionanotechnology.⁹⁻¹¹

Molecular dynamics (MD) provides an alternative approach for studying the dynamic interaction of fullerenes with cells in molecular-level detail. Previous atomistic simulation studies of bacterial membranes have shown that timescales required to observe penetration into these resilient membranes necessitates the use of coarse-grain (CG) MD.^{12,13} In fact, simulations have shown that the translocation of pristine C₆₀ fullerenes through even the simplest of phospholipid bilayers can occur on a microsecond timescale, which is too demanding for conventional all-atom MD.¹⁴⁻¹⁷ Here we report CG MD simulations of the interaction of C₆₀ nanoparticles with model bacterial membranes. The membrane models are composed of lipopolysaccharide (LPS) and palmitoyloleoylphosphoethanolamine (POPE) lipids. Through this series of CG simulations, we show that C₆₀ fullerene translocation depends on specific lipid composition. The fullerenes have a limited tendency to penetrate bacterial

1
2
3 membranes whose major component is Re mutant LPS i.e. the minimal biologically
4 active structure of endotoxins,¹⁸ which consists of lipid A and two molecules of 3-
5 deoxy-D-manno-2octulosonic acid (KDO), but the translocation of C₆₀ fullerenes into
6 bilayers whose major component is Ra LPS, which contains additional peripheral
7 head group sugars (Figure 1),¹⁹ is an energetically unfavorable process. Moreover,
8 we show that C₆₀ fullerenes more frequently penetrate Re LPS bilayers when they
9 are loaded with ions of low charge, when they are heated to a high temperature, or
10 when they incorporate small defect domains of POPE. The submerged fullerenes
11 tend to migrate to the interface between coexisting lipid fractions, where they
12 promote lipid mixing by reducing the line tension between the separate bilayer
13 domains. The differing permeabilities of the Re LPS bilayers are rationalized in terms
14 of their translocation mechanism, which involves the localized expansion of lipids
15 adjacent to C₆₀ molecules at the membrane interface.
16
17
18
19
20
21
22
23
24
25
26
27
28

29 **Experimental**

30 **CG models of LPS**

31
32 The models of LPS (at the Re and Ra levels) are similar to those reported by Ma et al.
33 and Van Oosten et al.^{20,21} Small modifications were made to improve the accuracy of
34 the models based on our own united-atom (UA) simulations. The mappings used for
35 the CG models, and the chemical structure of the UA models from which they were
36 parameterized are shown in Figure 1.
37
38
39
40
41
42
43
44
45
46
47
48
49
50
51
52
53
54
55
56
57
58
59
60

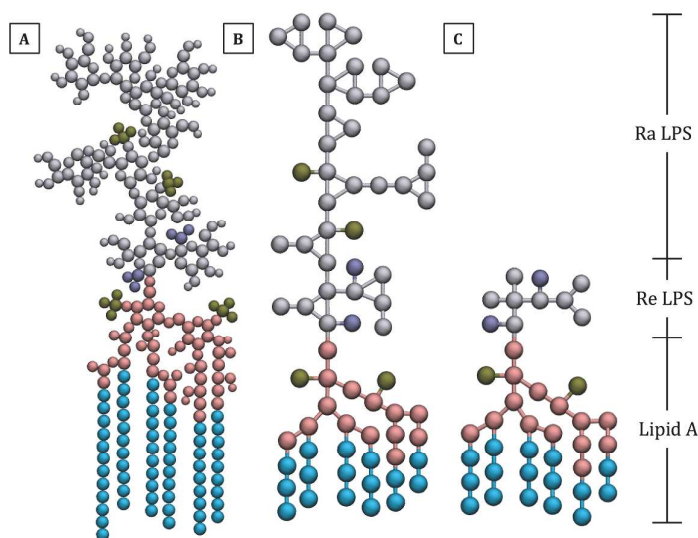


Figure 1: CG mapping schemes for Re and Ra LPS (A) The UA model for Ra LPS is shown alongside the CG model for (B) Ra LPS, and (C) Re LPS. Carbon tails are colored cyan, phosphate groups are colored brown, carboxylate groups are colored dark blue, glucosamine and glycerol groups are colored pink, and the remaining core saccharide sections are colored silver.

We analyzed lipid organization in the comparable UA and CG *E. coli* bacterial membranes by computing one-dimensional partial mass densities of lipid components along the bilayer normal (Figure 2). The peaks of the carbon tails, inner core sugars, and glucosamine and glycerol groups are equivalent to within 0.3 nm for both Re and Ra LPS, the outer core sugar peaks differ by ~ 0.4 nm. These simulations were performed with periodic boundary conditions throughout, ensuring that each lipid leaflet was in contact with similar solvent. The partial densities are discussed in terms of the Martini treatment of ions in more detail in the SI. Full details of the parameterization and validation of the CG models of LPS used here are provided in the supplementary information (Figure S1-S2, Table S1-S9).

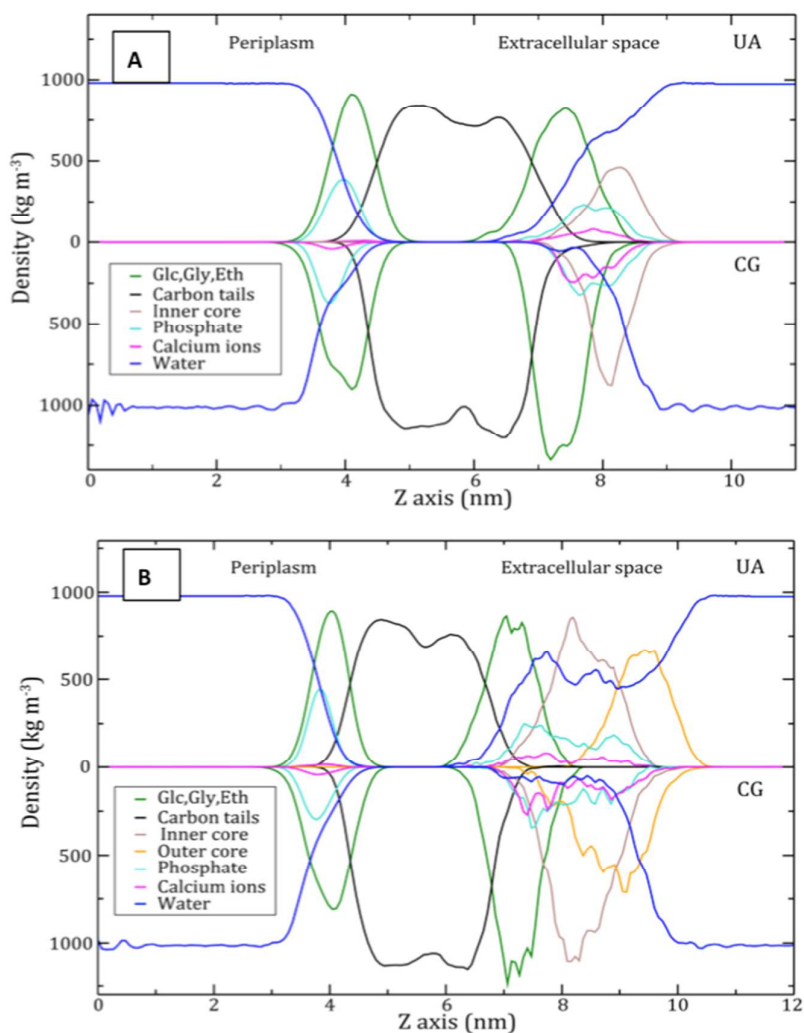


Figure 2: Comparative partial mass density plots for *E. coli* outer membranes. *E. coli* membranes were simulated at 310 K using CG and UA representations. The first membrane was built with a leaflet of (A) Re LPS, while the second membrane contained a leaflet of (B) Ra LPS instead. Carbon tails are represented by black lines, glucosamine, glycerol and ethanolamine groups (Glc,Gly,Eth) are represented by green lines, phosphate groups are represented by turquoise lines, calcium ions are represented by pink lines, inner core sugars are represented by brown lines, outer core sugars are represented by orange lines, and water is represented by blue lines. The partial mass densities are measured along the bilayer normal (Z axis).

CG simulation systems and protocols

The CG membranes were placed in the center of a periodic box and immersed in standard Martini CG water and ions. The systems were energy minimized with the steepest decent algorithm, and subsequently simulated at constant temperature and pressure. Model membranes were composed of (i) only LPS and (ii) LPS with small defect domains of POPE. POPE is the most abundant phospholipid in Gram-negative membranes and has been found in small concentrations in the outermost LPS leaflets as a stress response for LPS mutants of complete core saccharide section, and among incomplete core LPS mutants under standard conditions.^{22,23} In each instance, the membranes were solvated with CG water, anions (Cl^-) and cations (Ca^{2+} or Na^+) and subsequently simulated for 5 μs , to converge the lipid properties. Divalent cations are essential for retaining the integrity of LPS-containing leaflet as they cross-link the head groups.²⁴ We used a symmetric bilayer instead of an asymmetric model of the outer membrane purely for reasons of computational pragmatism. We did not want the C_{60} to cross the periodic boundaries and insert via the more penetrable inner leaflet given that our main focus is the interaction with the LPS-containing leaflet. The temperature was maintained at either 310 or 325 K using the velocity-rescaling thermostat²⁵ with a relaxation time of 4 ps, while the pressure was maintained at 1 bar through semi-isotropic coordinate scaling with the Parrinello-Rahman barostat^{26,27} and a time constant of 12 ps. The higher temperature of 325K was used to enable greater coverage of the phase space, rather than for biological relevance. The non-bonded interactions were cut off at a distance of 1.2 nm. The Lennard-Jones, and Coulomb potentials were shifted from 0.9 and 0.0 nm to the cutoff distance, respectively. The equations of motion were integrated with a 10 fs time step. Following this, the bilayers were brought into contact with different concentrations of CG C_{60} fullerenes to provide a comprehensive account of how monomeric and clustered C_{60} fullerenes interact with model bacterial membranes. The CG C_{60} fullerenes were described with a parameter set that was optimized to reproduce partitioning free energies for fullerenes between different organic solvents.²⁸ The simulations were performed with the GROMACS simulation package (version 4.5.5), and the Martini force field (version 2.2). Molecular graphic

1
2
3 images and trajectories were visualized with Visual Molecular Dynamics (VMD)
4 software.²⁹
5
6
7

8 **Analyses of the unrestrained C₆₀ fullerene simulations**

9
10 Contact analysis was performed with the *g_mindist* utility of GROMACS using a 0.6
11 nm cutoff distance. The position of molecules along the bilayer normal was
12 determined with the *g_traj* function. Two-dimensional partial mass density
13 landscapes were generated with a modified version of the *g_density* tool.³⁰
14
15
16
17

18 **Umbrella sampling simulations**

19
20 C₆₀ monomers were restrained at distances from the center of homogeneous
21 membranes using a harmonic potential, a force constant of 1000 KJ mol⁻¹ nm⁻² was
22 used for the biasing potential in the direction of the bilayer normal. The distance
23 between the fullerene and the center of the bilayer was decreased from a distance
24 of 5.2 nm to 0 nm, using 0.2 nm increments. Each umbrella sampling simulation was
25 1 μs long; the simulation temperature was 310 K throughout. All other simulation
26 parameters were set to match those of the unrestrained MD simulations.
27
28
29
30
31
32
33
34

35 **Results and Discussion**

36 **Unrestrained MD simulations**

37
38 To understand how fullerenes affect the outer membrane of Gram-negative
39 bacteria, we performed simulations to understand how pristine C₆₀ nanoparticles
40 interact with pure membranes of LPS, and membranes of LPS with small defect
41 domains of POPE. In each instance, the membranes had equivalent lipid distributions
42 in either leaflet, to ensure that the initial C₆₀-membrane interaction remained much
43 the same if the fullerenes happened to cross a boundary of the periodic box. The
44 series of simulations covered a range of different fullerene concentrations, providing
45 a comprehensive account of how both monomeric, and clustered fullerenes interact
46 with bacterial LPS. The lowest C₆₀ concentration was 0.01 mM, and the highest was
47 1.13 mM; experimental studies suggest that C₆₀ fullerenes are antibacterial towards
48
49
50
51
52
53
54
55
56
57
58
59
60

1
2
3 *E. coli* at concentrations as low as 0.06 mM.⁵ Tables S10 and Table S11 provide
4 additional details for these simulations, including the numbers of C₆₀ fullerenes per
5 periodic box, structural properties for the lipid bilayers, and the numbers of C₆₀
6 fullerenes that bypassed the phosphate boundary during the MD simulations.
7
8
9

10 11 12 **Pure LPS membranes**

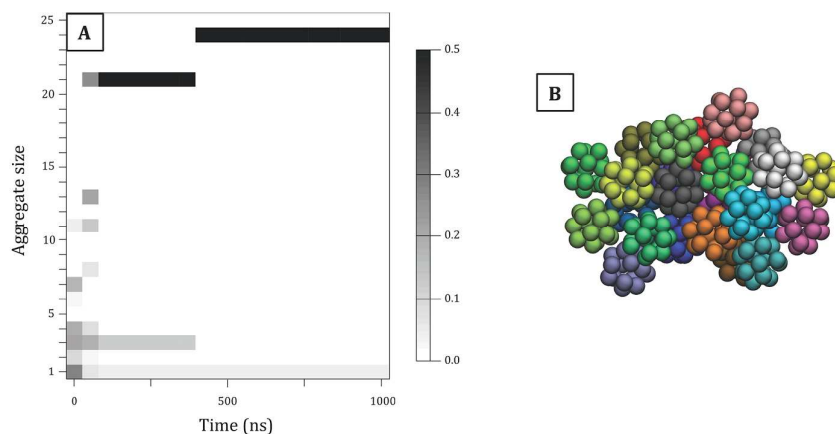
13 The first set of simulations explored how individual fullerenes interact with
14 membranes containing only Re or Ra LPS. The simulations were performed at both
15 CG and UA levels of detail, to provide a comparison for the different resolution levels
16 (details of the UA simulation conditions are provided in the supplementary
17 information). In the first part of the C₆₀ monomer simulations, the fullerenes
18 traversed the extracellular space (modeled as water and ions), and subsequently
19 latched onto the peripheral saccharide sections of LPS. From there on, the fullerenes
20 remained at the water-core sugar interface, displaying little lateral or vertical
21 movement. For the Re LPS bilayers, the fullerenes maintained a height of 0.92 ± 0.11
22 nm above the phosphate interface in the UA simulation, and 1.00 ± 0.06 nm in the
23 comparative CG system (sampling the last 100 ns of simulation time). In comparison,
24 the C₆₀ monomers maintained heights of 3.32 ± 0.16 nm in the UA simulation system
25 with Ra LPS, and 2.19 ± 0.04 nm for the analogous CG setup (Figure S3). The
26 mismatch in data for the Ra LPS system reveals the major deficiency of our CG LPS
27 parameterization and its implication for simulations with C₆₀: the height of the
28 peripheral core saccharide sections differs between the UA and CG membranes,
29 making the initial interactions between C₆₀ and Ra LPS different for the two
30 resolution levels.
31
32
33
34
35
36
37
38
39
40
41
42
43
44
45

46
47 The low permeability of the LPS bilayers to monomeric fullerenes stands in stark
48 contrast to the efficient solubilizing properties of most phospholipid membranes,
49 which readily dissolve large amounts of C₆₀ and C₇₀ fullerenes.³¹⁻³³ This seemingly
50 anomalous behavior could be attributed to the presence of densely packed core
51 sugars in the LPS head group region, or alternatively to differences in the
52 hydrophobic core of LPS and phospholipid bilayers. In either case, the translocation
53 of C₆₀ fullerenes into the bilayers should occur more frequently at higher
54
55
56
57
58
59
60

1
2
3 temperatures. To test if an increased simulation temperature would enable C_{60}
4 translocation we repeated the C_{60} monomer simulations at 325 K. At this
5 temperature, the Re LPS lipids frequently formed small cavities at the phosphate
6 interface whose size was comparable to that of the C_{60} fullerenes. As the fullerenes
7 came into contact with these transitory micropores, they slipped past the hydrophilic
8 head barrier, and thereby accessed the lipid core. Thereafter, the nanoparticles
9 dispersed among the encompassing lipid tails, maintaining a distance of
10 approximately 1 nm from the bilayer center (Figure S4). This mimics the positions
11 that fullerenes occupy in generic palmitoyloleoylphosphatidylcholine (POPC) and
12 dipalmitoylphosphatidylcholine (DPPC) lipid bilayers,^{34,35} this similarity in C_{60}
13 trajectories has been ascribed to higher acyl chain densities in this part of the bilayer.
14 In contrast, the Ra LPS membrane permeability was seemingly unchanged: the C_{60}
15 fullerenes did not penetrate the core sugar envelope to access the hydrophobic core
16 regardless of system temperature.
17
18
19
20
21
22
23
24
25
26
27
28

29
30 For the high concentration simulations (0.47 and 1.13 mM C_{60}) the nanoparticles
31 aggregated in the extracellular space to form globular clusters, that match nanosized
32 C_{60} crystals observed in transmission electron microscopy studies.³⁶ We explored the
33 clustering of the nanoparticles in terms of size and lifetime of C_{60} aggregates, the
34 analysis was performed by measuring the distances between C_{60} fullerenes during
35 the CGMD simulations. Whenever this separation distance was smaller than 1.3 nm,
36 the molecules were defined as clustered. The selected cutoff distance (1.3 nm) is
37 comparable to maximums in dimerization free energy profiles for CG C_{60} models in
38 different polar and apolar solvents and thus seems a sensible metric for
39 aggregation.³⁷ Our results revealed that C_{60} fullerenes form structures at least 5 nm
40 wide, within the first 400 ns of simulation time (Figure 3). Once clustered, the
41 fullerenes remained in an aggregated state as they latched onto the peripheral
42 saccharide sections of Re and Ra LPS. But despite their large size, the C_{60} aggregates
43 had negligible effect on the dynamic properties of the membrane. Lipid surface area
44 changed by less than 0.02 nm^2 , membrane thickness changed by less than 0.2 nm,
45 and there was only a minute modification of lipid order (Table S10). The small
46 perturbation of bilayer structural parameters in the various fullerene simulations
47
48
49
50
51
52
53
54
55
56
57
58
59
60

1
2
3 suggests that direct mechanical damage (e.g. bilayer rupture, or the formation of
4 pores) is not responsible for the antibacterial effects of C₆₀.
5
6

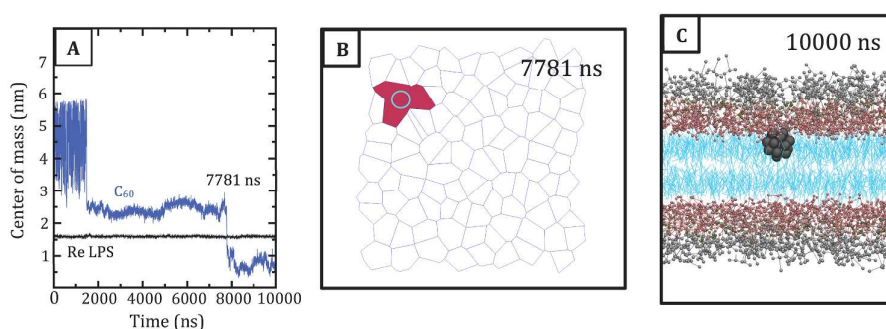


7
8
9
10
11
12
13
14
15
16
17
18
19
20
21
22
23 **Figure 3: Clustering of C₆₀ in a representative CG simulation** (A) The clustering of C₆₀
24 is plotted as a function of time during the first 1 μs of a CG simulation. The grayscale
25 in each cell represents the fraction of C₆₀ involved in an aggregate of a given size (y
26 axis) at a given time (x axis). The C₆₀ concentration was 1.13 mM. (B) Snapshot of the
27
28 24-unit C₆₀ cluster formed toward the end of this initial period of aggregation.
29
30
31
32

33 Simulations with sodium ions

34
35 Given that LPS leaflets display markedly different properties in the presence of
36 different cations, we explored how fullerenes would interact with LPS membranes in
37 the presence of (standard CG Martini) monovalent sodium ions (in place of the
38 calcium ions used before). Similar to results from atomistic simulation and
39 experimental studies, the LPS leaflets seemed more penetrable when they were
40 loaded with ions of low charge.^{38,39} The monovalent cations were less able to screen
41 the repulsive electrostatic interactions between the neighboring molecules of LPS,
42 which lead to increased lateral expansion within the bilayer plane. The Re LPS area
43 per lipid increased from a value of $1.58 \pm 0.00005 \text{ nm}^2$ to a value of 1.70 ± 0.0001
44 nm^2 at 310 K, while the membrane thinned from a thickness of $3.39 \pm 0.0001 \text{ nm}$ to
45 $3.25 \pm 0.0002 \text{ nm}$. Evidently, the Re LPS bilayers present a less formidable barrier in
46 the presence of monovalent cations, and as a consequence, the C₆₀ fullerenes more
47 readily entered the Re LPS bilayer core. This is evident for the simulations performed
48 at the lower, biologically relevant temperature of 310 K (Table S11), where C₆₀
49
50
51
52
53
54
55
56
57
58
59
60

1
2
3 fullerenes successfully bypassed the LPS head group barrier, to access the lipid core.
4 The translocation occurred as C_{60} monomers came into contact with transient
5 micropores. Two-dimensional voronoi tessellations of the membrane surface show
6
7 micropores. Two-dimensional voronoi tessellations of the membrane surface show
8 that the micropores were the product of localized lateral expansion of the Re LPS
9 bilayer. One of these micropores was formed as three LPS lipids expanded within the
10 bilayer plane to increase the local area per lipid from a value of $1.70 \pm 0.0001 \text{ nm}^2$ to
11 2.02 nm^2 , and in so doing, temporarily establish a cavity in the bilayer surface (Figure
12 4).
13
14
15
16
17
18
19



20
21
22
23
24
25
26
27
28
29
30
31
32 **Figure 4: The effect of sodium ions on Re LPS bilayer permeability.** (A) Position of
33 the C_{60} monomer along the bilayer normal, relative to the Re LPS bilayer center. The
34 blue line depicts the center of mass coordinates for the C_{60} monomer from the
35 bilayer center, while the black line shows the average position of LPS boundary
36 phosphate groups in a single leaflet of the bilayer. The simulation was performed at
37 310 K, with a single C_{60} fullerene. (B) Two-dimensional voronoi tessellation of the Re
38 LPS surface as the C_{60} fullerene bypasses the phosphate barrier at 7781 ns. Each cell
39 represents a single Re LPS head group. The red cells correspond to the LPS head
40 groups adjacent to the C_{60} monomer. The cyan circle shows the position of the C_{60}
41 monomer during the head group tunneling event. (C) Side-view snapshot for the C_{60}
42 monomer after it bypassed the phosphate interface to settle in the lipid core.
43
44
45
46
47
48
49
50
51
52

53 The formation of transient micropores via localized lateral lipid expansion facilitates
54 the insertion of monomeric C_{60} fullerenes into the Re LPS bilayer core, but larger
55 multimeric clusters were unable to bypass the phosphate boundary. As a
56
57
58
59
60

1
2
3 consequence, there was only partial embedding of C₆₀ fullerenes into the Re LPS
4 membrane when the fullerene concentration was increased from 0.02 mM, to 0.35
5 mM. At this concentration, most of the fullerene monomers had tunneled through
6 hydrophobic pores to access the lipid core, while the larger globular clusters
7 interacted with the peripheral LPS saccharide domain.
8
9

10
11
12
13 For the Ra LPS bilayer, the area per lipid increased from $1.83 \pm 0.00004 \text{ nm}^2$ at 310 K,
14 to $1.95 \pm 0.00004 \text{ nm}^2$ as the calcium ions were exchanged for less polar sodium
15 ions. But despite the changes in the structural properties of the membrane, the C₆₀
16 fullerenes were unable to pass through the phosphate interface.
17
18
19

20 21 22 **Mixed lipid membranes**

23
24 Given that the endotoxin (LPS) leaflet of bacterial outer membranes can incorporate
25 small phospholipid defect domains *in vivo*,⁴⁰⁻⁴³ we explored the possibility that C₆₀
26 preferentially interacts with these lipids over (both Re and Ra) LPS. We replaced
27 approximately 25% of the LPS membrane surface with small clusters of POPE lipids.
28 The clusters covered a range of different sizes ranging from 10 to 25 POPE lipids.
29 Similar to the results from experimental studies,^{22-23,44} the POPE lipids tended to
30 separate from the encompassing LPS, dividing the membrane into two distinct
31 sections. After the dual component membranes had divided into distinct fractions,
32 they were brought into contact with a range of different fullerene concentrations.
33
34
35
36
37
38
39

40
41
42 The incorporation of POPE lipids made the membranes more penetrable to the C₆₀
43 nanoparticles. At low concentrations, fullerene monomers accessed the membrane
44 cores more frequently (per simulation) as they passed through the POPE
45 headgroups. After inserting into the lipid core, the monomers traversed the acyl tail
46 section, staying at least 0.5 nm from the bilayer center.
47
48
49
50
51
52
53
54
55
56
57
58
59
60

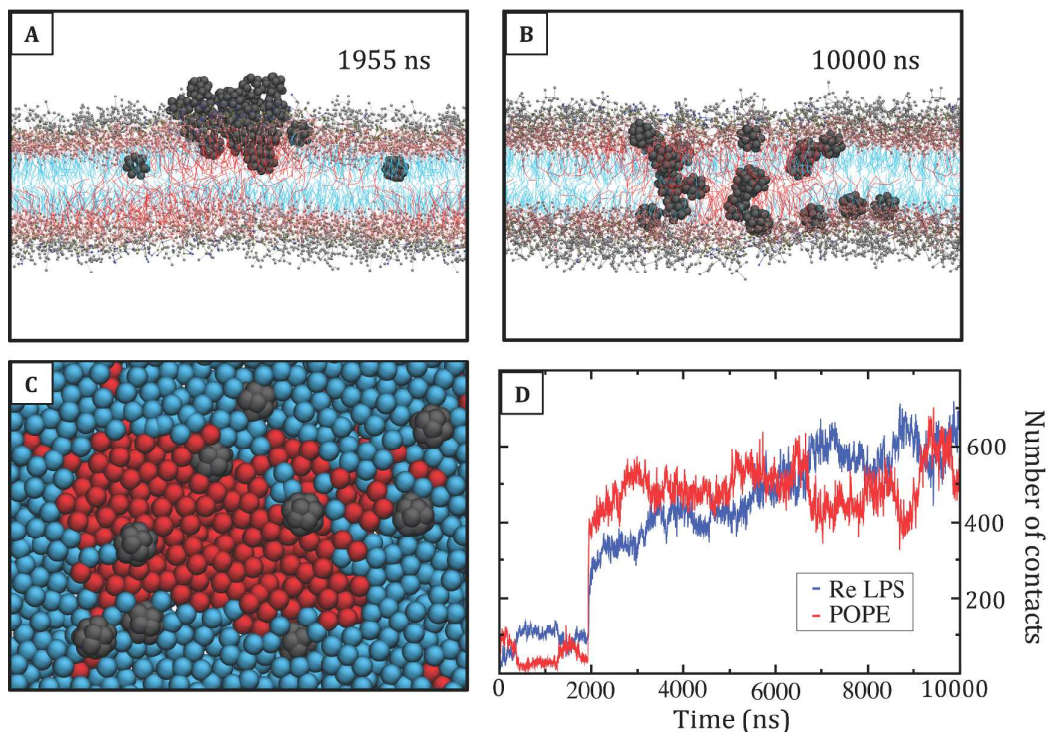


Figure 5: Migration of C₆₀ fullerenes to the POPE-Re LPS lipid interface. (A) The C₆₀ cluster migrates to the domain of POPE, and slips past the hydrophilic head groups to access the lipid core. (B) The cluster disaggregates, and the disbanded fullerenes drift to the interface between the separate POPE and LPS domains. The Re LPS are colored as before, and the POPE lipid tails are colored red. (C) Top-view snapshot of the disbanded fullerenes at the POPE-Re LPS lipid interface. The lipid head groups are omitted for clarity. (D) The number of contacts between the C₆₀ fullerenes and the (Re LPS and POPE) acyl tails is plotted as a function of simulation time. The red line shows the number of contacts between the fullerenes and POPE lipid tails, while the blue shows the number of contacts between the fullerenes and the Re LPS lipid tails. The relative number of contacts was determined using a 0.6 nm cutoff distance.

1
2
3
4
5 For the high concentration simulations (0.37 mM and 0.66 mM), the nanosized C₆₀
6 clusters were likewise capable of penetrating the multicomponent membranes.
7
8 Initially, the fullerene monomers coalesced to form globular clusters within the first
9
10 300 ns of simulation time. After that, the C₆₀ aggregates migrated to the POPE lipids
11 and passed through their head groups, or alternatively they remained atop the
12 peripheral saccharide section of LPS (Figure 5A,B). We explored how this insertion
13 event took place through the use of two-dimensional projections of phosphate and
14 choline mass densities, voronoi tessellations of LPS and POPE head group atoms, and
15 separation distance calculations. By partitioning the membrane surface into distinct
16 domains based on local area per lipid and local particle densities, we resolved the
17 translocation process. At the moment of insertion, approximately 10 POPE
18 headgroups moved apart to create a micropore whose shape and surface area
19 matched those of the C₆₀ aggregate (Figure 6). The POPE area per lipid value
20 approached 2.0 nm² during this time (Figure 6F), while the POPE width increased by
21 approximately 10 %. These local deforming effects were gradually suppressed as the
22 cluster subsequently broke apart, and the disconnected C₆₀ monomers dispersed
23 among the surrounding lipid tails. Similar disaggregation behavior has been noted in
24 phospholipid bilayers, and rationalized as the result of high carbon atom densities,
25 and the perturbation of chain packing by the fullerene clusters.⁴⁵
26
27
28
29
30
31
32
33
34
35
36
37
38
39
40
41
42
43
44
45
46
47
48
49
50
51
52
53
54
55
56
57
58
59
60

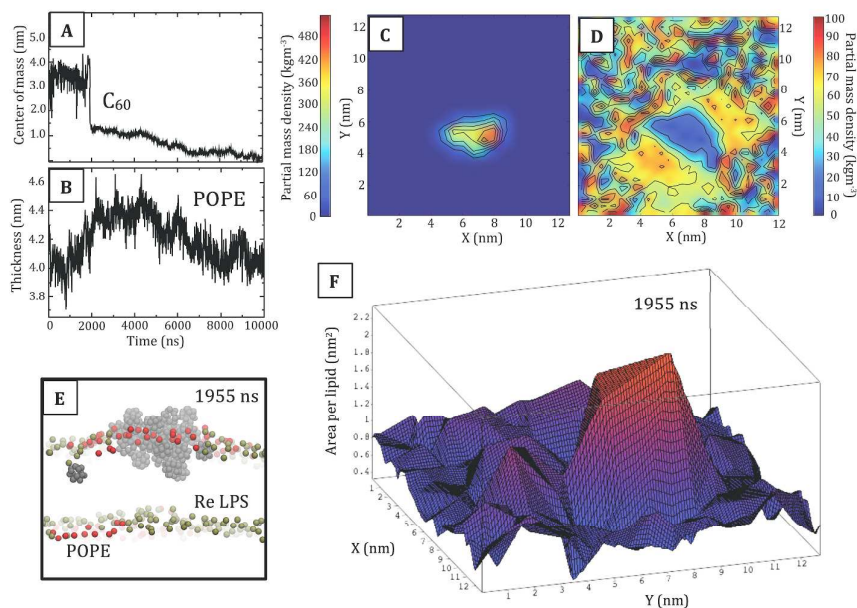


Figure 6: Translocation of a C₆₀ cluster across the water-lipid interface. (A) Average center of mass coordinates for C₆₀ fullerenes along the bilayer normal (relative to the bilayer center). (B) Average thickness of the POPE lipids plotted against simulation time; thickness was defined as the distance between POPE phosphate head groups and the bilayer center. (C) Two-dimensional partial mass density for C₆₀ fullerenes comprising the C₆₀ cluster, during the bilayer insertion event (1955 ns). (D) Partial mass densities for Re LPS phosphate and POPE choline head groups during fullerene cluster insertion (1955 ns). The POPE head groups move apart to create a transient micropore whose shape and projected surface area match those of the C₆₀ cluster. (E) Side-view snapshot of the C₆₀ cluster traversing the phosphate interface, the Re LPS phosphate groups are colored brown, the POPE phosphate groups are colored red. All other membrane components are omitted for clarity. (F) Three-dimensional projection of area per lipid values for the membrane leaflet that the C₆₀ fullerenes pass through. The tessellation was performed for the membrane surface at 1955 ns. Red color represents high area per lipid while blue color represents low area per lipid.

Towards the end of the CG simulations, the disconnected monomers accumulated at the interfacial regions between the Re LPS and POPE domains. This was discerned by

1
2
3 calculating contact numbers for the C₆₀ fullerenes and the carbon tails of the dual-
4 component bilayer (using a 0.6 nm cutoff distance). The number of contacts
5 between the POPE lipid tails and C₆₀ fluctuated about an average value once the
6 fullerenes had passed through the phosphate interface, while the number of
7 contacts between the Re LPS tails and the fullerenes initially increased, before
8 converging to a definite value. The results indicate that the C₆₀ fullerenes were
9 migrating towards the interfacial regions of the multicomponent membranes during
10 the course of the MD simulation. The behavior is reminiscent of linactants,⁴⁶⁻⁴⁹ which
11 tend to collect at the interface between liquid-ordered and liquid-disordered
12 domains, and promote lipid mixing by destabilizing the phase boundary. To explore
13 the possibility that the embedded fullerenes were affecting the boundaries between
14 the separate domains of Re LPS and POPE, we calculated how lipid properties
15 changed in the presence of the fullerenes. In particular, we focused on the
16 simulations with complete immersion of all available C₆₀ fullerenes in the bilayer
17 core, to remove any extraneous influence of fullerene clusters binding to the
18 peripheral saccharide section of LPS. We found that the dispersion of C₆₀ fullerenes
19 in the lipid core lead to greater homogeneity of lipid properties for the separate LPS
20 and POPE domains. There was a general reduction in the mismatch of bilayer
21 thickness, lipid order, and area per lipid, which lead to a reduction in the line tension
22 (boundary free energy) between the coexisting lipid fractions. For example, the
23 thickness mismatch decreased by 0.2 nm when 25 fullerenes were introduced into
24 the core of the membrane with Re LPS and POPE (Figure 7). The changes in lipid
25 properties suggest that the fullerenes were promoting lipid mixing and encouraging
26 the formation of a more uniform membrane.
27
28
29
30
31
32
33
34
35
36
37
38
39
40
41
42
43
44
45
46
47
48
49
50
51
52
53
54
55
56
57
58
59
60

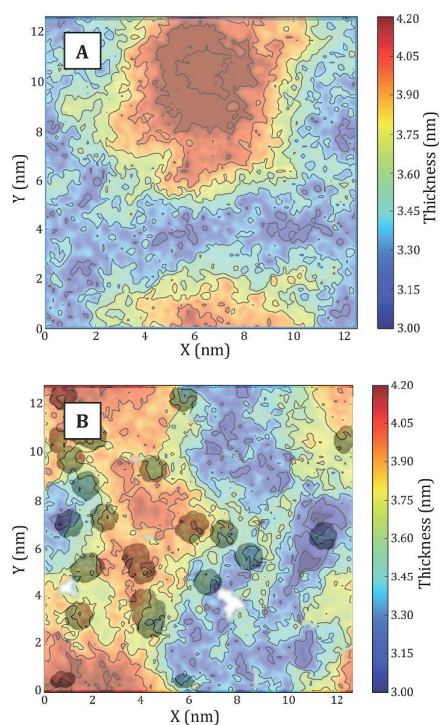


Figure 7: C₆₀ fullerenes promote lipid mixing in the multicomponent membrane.

After the C₆₀ fullerenes had entered the bilayer core, they migrated to the boundaries between the coexisting POPE and Re LPS domains. The fullerenes then reduced the line tension between the coexisting lipid fractions by minimizing structural mismatch. The figures depict the bilayer thickness as a two-dimensional landscape for the membrane (A) without any C₆₀ fullerenes dissolved in the lipid core, and (B) with 25 C₆₀ fullerenes dispersed among the lipid tails. The final C₆₀ particle positions are depicted above the thickness landscape as translucent black spheres (for reference).

Free energy profiles

Given the diverse interactions between C₆₀ fullerenes and the LPS bilayers observed in the unrestrained MD simulations, we calculated potential of mean force (PMF) profiles to better understand the different bilayer permeabilities. Single C₆₀ fullerenes were restrained at different distances from homogeneous bilayers of Re LPS, Ra LPS, and POPE in the presence of either monovalent sodium ions (Na⁺), or divalent calcium ions (Ca²⁺). The weighted histogram analysis method was

1
2
3 subsequently utilized to produce a collection of PMF profiles, which are shown in
4 Figure 8. The analysis reveals that C_{60} translocation is thermodynamically favored for
5 POPE and Re LPS bilayers regardless of ambient ion type, but the translocation of C_{60}
6 fullerenes into Ra LPS bilayers is energetically unfavorable. The data show that
7 increasing the length of the LPS core sugar section can profoundly influence the
8 thermodynamics of C_{60} translocation, and likewise suggests that phospholipid defect
9 domains can make LPS containing bilayers permeable to C_{60} fullerenes. Moreover,
10 the PMF profiles help to clarify fullerene trajectories in the Re LPS and POPE lipid
11 core. The PMF profiles have (global) free energy minima at distances of
12 approximately 0.5 and 1.5 nm from the bilayer center for the Re LPS and POPE
13 bilayers, respectively. These energy minima reveal that it is more favorable for the
14 C_{60} nanoparticles to settle among the high density Re LPS lipid tails than the bilayer
15 center, explaining the tendency for C_{60} fullerenes to avoid the bilayer center in the
16 unrestrained MD simulations.

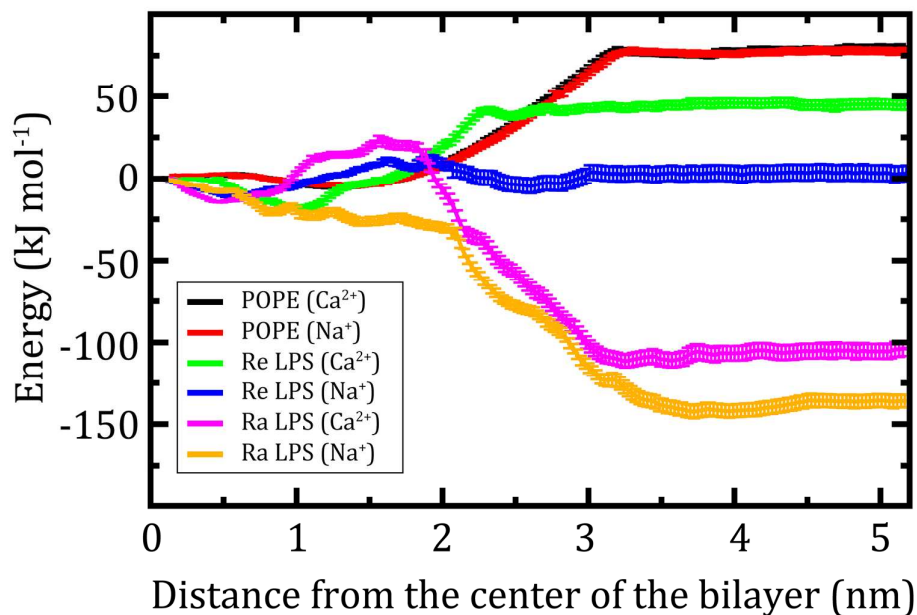


Figure 8: PMF profiles for C_{60} fullerene as a function of distance from the center of homogeneous lipid bilayers. PMF profiles for C_{60} fullerene as a function of distance from the bilayer center. The red line shows the data for the POPE bilayer with Na^+

1
2
3 ions, the black line shows the data for the POPE bilayer with Ca^{2+} , the green line
4 shows the data for the Re LPS bilayer with Ca^{2+} ions, the blue line shows the data for
5 the Re LPS bilayer with Na^+ , the pink line shows the data for the Ra LPS bilayer with
6 Ca^{2+} ions, and the orange line shows the data for the Ra LPS bilayer with Na^+ ions.
7
8 Each umbrella sampling simulation was 1 μs long; the simulation temperature was
9
10 310 K; the umbrella sampling windows were separated by distances of 0.2 nm. The
11
12 free energy was set to zero at the bilayer center.
13
14

15 16 17 **Conclusion** 18

19
20
21 A series of CG simulations was performed to better understand the interaction of C_{60}
22
23 fullerenes with the outer membrane of *E. coli*. We found that pristine C_{60} has a
24
25 limited tendency to penetrate homogeneous bilayers of (incomplete core
26
27 saccharide) Re LPS, but the translocation of C_{60} fullerenes into homogeneous
28
29 (complete core saccharide) Ra LPS bilayers is an energetically unfavorable process.
30
31 Secondly, we have shown that the permeability of Re LPS bilayers depends
32
33 sensitively on the charge of ambient ions, on the system temperature, and on the
34
35 prevalence of phospholipid defect domains (specifically POPE lipids) among the Re
36
37 LPS lipids. The differing permeabilities were rationalized in terms of transitory pore
38
39 formation at the phosphate interface, which was driven by localized lipid head group
40
41 expansion. The Re LPS molecules expanded readily to form large transient
42
43 micropores when they were interlinked with monovalent (rather than divalent)
44
45 cations, or when they were heated to a higher temperature, enabling the C_{60}
46
47 fullerenes to tunnel the phosphate interface more effectively. The POPE lipids were
48
49 most effective at forming large transient micropores, and their inclusion enabled the
50
51 formation of the largest transitory cavities that were tunneled by C_{60} fullerenes both
52
53 in their monomeric, and clustered form.
54

55
56 When inside the lipid core, the fullerenes behaved similarly to linactants: the
57
58 fullerenes moved to the interface between the separate POPE and LPS domains,
59
60 where they reduced the boundary free energy between the coexisting lipid fractions

1
2
3 by minimizing structural mismatch.⁵⁰ This reduction in the membrane line tension
4 could have important consequences for membrane lateral organization on larger-
5 scales, which is pertinent to various cellular processes such as signaling and protein
6 trafficking.
7
8
9

10
11 In conclusion, we have demonstrated that the interaction of C₆₀ fullerenes with the
12 *E. coli* outer membranes depends sensitively on ambient temperature; on the length
13 of the LPS core saccharide section; on the prevalence of phospholipid defect
14 domains and the charge of the ions that interlink LPS phosphate groups. The
15 incorporation of even small concentrations of phospholipids, single unit changes in
16 the charge density of stabilizing counterions, or minor modifications of the ambient
17 temperature ($\Delta T = 15$ K), can profoundly affect how fullerenes interact with bilayers
18 that contain LPS, and where they settle within the membrane. More interestingly,
19 the extension of the LPS core sugar section can change C₆₀ fullerene translocation
20 from being an energetically favorable process, to being energetically unfavorable.
21 The results help to explain why seemingly contradictory toxicological evaluations
22 have been obtained for C₆₀ and its different derivatives.⁵¹⁻⁵⁴ The mismatch may be
23 ascribed to small differences in temperature, ambient ion concentrations, LPS core
24 sugar length, or the prevalence of phospholipid defect domains leading to
25 significantly different interactions between the C₆₀ fullerenes and the Gram-negative
26 outer membranes. We have provided a comprehensive account of how fullerenes
27 bind to, and interact with LPS lipids when they are incorporated into membranes.
28 The molecular level insights from our simulations provide a rational starting point for
29 modifying fullerenes to increase their effectiveness as antibacterial agents.
30
31
32
33
34
35
36
37
38
39
40
41
42
43
44
45

46 47 **ASSOCIATED CONTENT**

48 49 **Supporting Information**

50 Four figures and eleven tables to validate the LPS parameters and provide additional
51 simulation data.
52
53
54

55 56 57 **AUTHOR INFORMATION**

Corresponding author

*Email: S.Khalid@soton.ac.uk. Tel.: +44-2380-594176. Fax: +44-2380-593781.

Acknowledgment

This project made use of time on ARCHER granted via the UK High-End Computing Consortium for Biomolecular Simulation, HECBioSim (<http://hecbiosim.ac.uk>), supported by EPSRC (grant no. EP/L000253/1). Computer code was developed was James Graham.

References

- 1 Kroto, H. W.; Heath, J. R.; O'Brien, S. C.; Curl, R. F.; Smalley, R. E. C₆₀: Buckminsterfullerene *Nature* **1985**, 318, 162-163.
- 2 Günes, S.; Neugebauer, H.; Sariciftci, N. S. Conjugated Polymer-Based Organic Solar Cells *Chem. Rev.* **2007**, 107, 1324-1338.
- 3 Mendes, R. G.; Bachmatiuk A.; Büchner, B.; Cuniberti, G.; Rummeli, M. H. Carbon Nanostructures as Multi-Functional Drug Delivery Platforms. *J. Mater. Chem. B* **2013**, 14, 401-428.
- 4 Montellano, A.; Da Ros, T.; Bianco, A.; Prato, M. Fullerene C₆₀ as a Multifunctional System for Drug and Gene Delivery. *Nanoscale* **2011**, 3, 4035-4041.
- 5 Lyon, D. Y.; Fortner, J. D.; Sayes, C. M.; Colvin, V. L.; Hughes, J. B. Bacterial Cell Association and Antimicrobial Activity of a C₆₀ Water Suspension. *Environ. Toxicol. Chem.* **2005**, 24, 2757-2762.
- 6 Lyon, D. Y.; Brown, D. A.; Alvarez, P. J. J. Implications and Potential Applications of Bactericidal Fullerene Water Suspensions: Effect on nC₆₀ Concentration, Exposure Conditions and shelf Life. *Water Sci. Technol.* **2008**, 57, 1533-1538.
- 7 Ma, Y. Q. Theoretical and Computational Studies of Dendrimers as Delivery Vectors. *Chem. Soc. Rev.* **2013**, 42, 705-727.

- 1
2
3 8 Ding, H. M.; Ma, Y. Q. Theoretical and Computational Investigations of
4 Nanoparticle-Biomembrane Interactions in Cellular Delivery. *Small* **2015**, 11,
5 1055-1071.
6
7
8 9 Fortner, J. D.; Lyon, D. Y.; Sayes, C. M.; Boyd A. M.; Falkner, J. C.; Hotze, E. M.;
9
10 Alemany, L. B.; Tao, Y. J.; Guo, W.; Ausman, et al. C₆₀ in Water: Nanocrystal
11 Formation and Microbial Response. *Environ. Sci. Technol. Lett.* **2005**, 39, 4307-
12 4316.
13
14 15 Lyon, D. Y.; Alvarez. P. J. J. Fullerene Water Suspension (nC₆₀) Exerts
16 Antibacterial Effects via ROS-Independent Protein Oxidation. *Environ. Sci.*
17 *Technol. Lett.* **2008**, 42, 8127-8132.
18
19 20 Brunet, L.; Lyon, D. Y.; Hotze, E. M.; Alvarez, P. J.; Wiesner, M. R. Comparative
21 Photoactivity and Antibacterial Properties of C₆₀ Fullerenes and Titanium
22 Dioxide Nanoparticles. *Environ. Sci. Technol.* **2009**, 43, 4355-4360.
23
24 25 Berglund, N. A.; Piggot, T. J.; Jefferies, D.; Sessions, R. B.; Bond, P. J.; Khalid, S.
26 Interaction of the Antimicrobial Peptide Polymyxin B1 with Both Membranes
27 of *E. coli*: a Molecular Dynamics Study. *PLoS Comput. Biol.* **2015**, 11,
28 e1004180.
29
30 31 Sansom, M. P.; Scott, K.; Bond, P. Coarse-Grained Simulation: a High-
32 Throughput Computational Approach to Membrane Proteins. *Biochem. Soc.*
33 *Trans.* **2008**, 36, 27-32.
34
35 36 Chen, K.; Ma, Y. Q. Interaction of Fullerene Chains and a Lipid Membrane via
37 Computer Simulations. *RSC Adv.* **2014**, 4, 30215-20.
38
39 40 D’Rozario, R. S.; Wee, C. L.; Wallace, E. J.; Sansom, M. S. The Interaction of
41 C60 and its Derivatives with a Lipid Bilayer via Molecular Dynamics
42 Simulations. *Nanotechnol.* **2009**, 20, 115102.
43
44 45 Wong-Ekkabut, J.; Baoukina,S.; Triampo, W.; Tang, I. M.; Tieleman, D. P.;
46 Monticelli, L. Computer Simulation Study of Fullerene Translocation Through
47 Lipid Membranes. *Nat. Nanotechnol.* **2008**, 3, 363-368.
48
49 50 DeVane, R.; Jusufi, A.; Shinoda, W.; Chiu, C. C.; Nielsen, S. O.; Moore, P. B.;
51 Klein, M. L. Parameterization and Application of a Coarse Grained Force Field
52 for Benzene/Fullerene Interactions with Lipids. *J. Phys. Chem. B* **2010**, 114,
53 16364-16372.
54
55
56
57
58
59
60

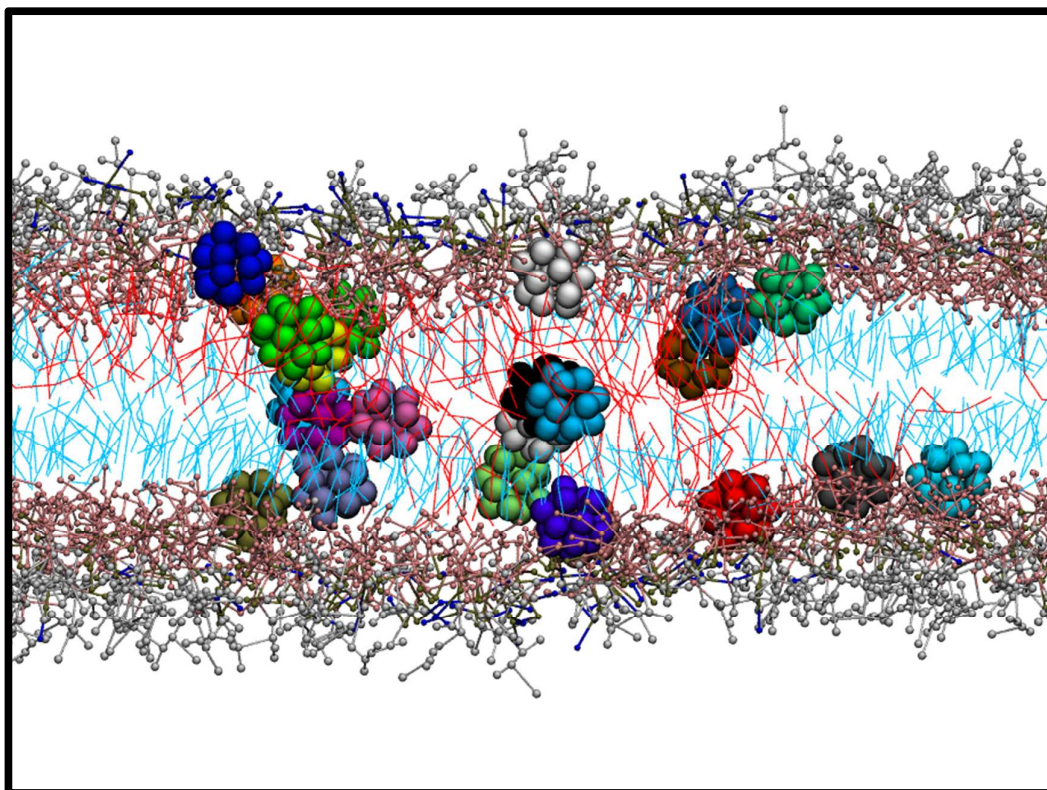
- 1
2
3 18 Zähringer, U.; Lindner, B.; Seydel, U.; Rietschel, E. T.; Naoki, H.; Unger, F. M.;
4 Imoto, M.; Kusumoto, S.; Shiba, T. Structure of De-O-acylated
5 Lipopolysaccharide from the *Escherichia Coli* Re Mutant Strain F 515.
6 *Tetrahedron Lett.* **1985**, 26, 6321-6324.
7
8
9
10 19 McIntire, F. C.; Sievert, H. W.; Barlow, G. H.; Finley, R. A.; Lee, A. Y. Chemical,
11 Physical, and Biological Properties of a Lipopolysaccharide from *Escherichia*
12 *Coli* K-235. *Biochemistry* **1967**, 6, 2363-2372.
13
14
15 20 Ma, H.; Irudayanathan, F. J.; Jiang, W.; Nangia, S. Simulating Gram-Negative
16 Bacterial Outer Membrane: a Coarse Grain Model. *J. Phys. Chem. B* **2015**, 119,
17 14668-14682.
18
19
20 21 Van Oosten, B.; Harroun, T. A. A MARTINI Extension for *Pseudomonas*
22 *Aeruginosa* PAO1 Lipopolysaccharide. *J. Mol. Graph.* **2016**, 63, 125-133.
23
24 22 Nikaido, H. Molecular Basis of Bacterial Outer Membrane Permeability
25 Revisited. *Microbiol. Mol. Biol. Rev.* **2003**, 67, 593-656.
26
27 23 Nikaido, H.; Vaara, M. Molecular Basis of Bacterial Outer Membrane
28 Permeability. *Microbiol. Rev.* 1985, 49, 1.
29
30 24 Clifton, L. A.; Holt, S. A.; Hughes, A. V.; Daulton, E. L.; Arunmanee, W.;
31 Heinrich, F.; Khalid, S.; Jefferies, D.; Charlton, T. R.; Webster, J. R. et al. An
32 Accurate in Vitro Model of the *E. Coli* Envelope. *Angew. Chem. Int. Ed.* **2015**,
33 54, 11 952-19955.
34
35
36 25 Szczelina, R.; Murzyn, K. DMG- α A Computational Geometry Library for
37 Multimolecular Systems. *J. Chem. Inf. Model.* **2014**, 54, 3112-3123.
38
39 26 Parrinello, M.; Rahman, A. Polymorphic Transitions in Single Crystals: a New
40 Molecular Dynamics Method. *J. Appl. Phys.* **1981**, 52, 7182-7190.
41
42 27 Nosé, S.; Klein, M. L. Constant Pressure Molecular Dynamics for Molecular
43 Systems. *Mol. Phys.* **1983**, 50, 1055-1076.
44
45 28 Monticelli, L. On Atomistic and Coarse-Grained Models for C₆₀ Fullerene. *J.*
46 *Chem. Theory Comput.* **2012**, 8, 1370-1378.
47
48 29 Humphrey, W.; Dalke, A.; Schulten, K. VMD: Visual Molecular Dynamics. *J.*
49 *Mol. Graph.* **1996**, 14, 33-38.
50
51
52
53
54
55
56
57
58
59
60

- 1
2
3 30 Castillo, N.; Monticelli, L.; Barnoud, J.; Tieleman, D. P. Free Energy of WALP23
4 Dimer Association in DMPC, DPPC, and DOPC Bilayers. *Chem. Phys. Lipids*
5 **2013**, 169, 95-105.
6
7
8 31 Ikeda, A.; Mori, M.; Kiguchi, K.; Yasuhara, K.; Kikuchi, J. I.; Nobusawa, K.;
9 Akiyama, M.; Hashizume, M.; Ogawa, T.; Takeya, T. Advantages and Potential
10 of Lipid-Membrane-Incorporating Fullerenes Prepared by the Fullerene-
11 Exchange Method. *Chem. Asian J.* **2012**, 7, 605.
12
13 32 Ikeda, A.; Sato, T.; Kitamura, K.; Nishiguchi, K.; Sasaki, Y.; Kikuchi, J. I.; Ogawa,
14 T.; Yogo, K.; Takeya, T. Efficient Photocleavage of DNA Utilizing Water-Soluble
15 Lipid Membrane-Incorporated [60] Fullerenes Prepared Using a [60] Fullerene
16 Exchange Method. *Org. Biomol. Chem.* **2005**, 16, 2907-2909.
17
18 33 Ikeda, A.; Doi, Y.; Nishiguchi, K.; Kitamura, K.; Hashizume, M.; Kikuchi, J. I.;
19 Yogo, K.; Ogawa, T.; Takeya, T. Induction of Cell Death by Photodynamic
20 Therapy with Water-Soluble Lipid-Membrane-Incorporated [60] Fullerene.
21 *Org. Biomol. Chem.* **2007**, 5, 1158-1160.
22
23 34 Monticelli, L.; Bozdaganyan, M. E.; Orekhov, P. S.; Shaytan, A. K.; Shaitan, K. V.
24 Comparative Computational Study of Interaction of C₆₀-Fullerene and Tris-
25 Malonyl-C₆₀-Fullerene Isomers with Lipid Bilayers: Relation to their
26 Antioxidant Effect. *PLOS ONE* **2014**, 9, e102487.
27
28 35 Bedrov, D.; Smith, G. D.; Davande, H.; Li, L. Passive Transport of C₆₀ Fullerenes
29 Through a Lipid Membrane: a Molecular Dynamics Simulation Study, *J. Phys.*
30 *Chem. B* **2008**, 112, 2078-2084.
31
32 36 Deguchi, S.; Alargova, R. G.; Tsujii, K. Stable Dispersions of Fullerenes, C₆₀ and
33 C₇₀, in Water Preparation and Characterization. *Langmuir* **2001**, 17, 6013-
34 6017.
35
36 37 Chiu, C. C.; DeVane, R.; Klein, M. L.; Shinoda, W.; Moore, P. B.; Nielsen, S. O.
37 Coarse-Grained Potential Models for Phenyl-Based Molecules: II. Application
38 to Fullerenes. *J. Phys. Chem. B* **2010**, 114, 6394-6400.
39
40 38 Snyder, S.; Kim, D.; McIntosh, T. J. Lipopolysaccharide Bilayer Structure: Effect
41 on Chemotype, Core Mutations, Divalent Cations, and Temperature.
42 *Biochemistry* **1999**, 38, 10758-10767.
43
44
45
46
47
48
49
50
51
52
53
54
55
56
57
58
59
60

- 1
2
3 39 Nascimento, A.; Pontes, F. J.; Lins, R. D.; Soares, T. A. Hydration, Ionic Valence
4 and Cross-Linking Propensities of Cations Determine the Stability of
5 Lipopolysaccharide (LPS) Membranes. *Chem. Commun.* **2014**, 50, 231-233
6
7
8 40 Nikaido, H. Permeability of the Lipid Domains of Bacterial Membranes. *Adv.*
9 *Membr. Fluid* **1990**, 4, 165-190.
10
11 41 Vaara, M.; Nurminen, M. Outer Membrane Permeability Barrier in *Escherichia*
12 *coli* Mutants that are Defective in the Late Acyltransferases of Lipid A
13 Biosynthesis, *Antimicrob. Agents Chemother.* **1999**, 43, 1459-1462.
14
15 42 Vaara, M. Antibiotic-Supersusceptible Mutants of *Escherichia Coli* and
16 *Salmonella Typhimurium*. *Antimicrob. Agents Chemother.* **1993**, 37, 2255.
17
18 **43** Smit, J. O.; Kamio, Y. O.; Nikaido, H. Outer Membrane of *Salmonella*
19 *Typhimurium*: Chemical Analysis and Freeze-Fracture Studies with
20 Lipopolysaccharide Mutants. *J. Bacteriol.* **1975**, 124, 942-958.
21
22 44 Kubiak, J.; Brewer, J.; Hansen, S.; Bagatolli, L. A. Lipid Lateral Organization on
23 Giant Unilamellar Vesicles Containing Lipopolysaccharides. *Biophys. J.* **2011**,
24 100, 978-986.
25
26 45 Barnoud, J.; Rossi, G.; Monticelli, L. Lipid Membranes as Solvents for Carbon
27 Nanoparticles, *Phys. Rev. Lett.* **2014**, 112, 068102.
28
29 46 Trabelsi, S.; Zhang, S.; Lee, T. R.; Schwartz, D. K. Linactants: Surfactant
30 Analogues in Two Dimensions. *Phys. Rev. Lett.* **2008**, 100, 037802.
31
32 47 Schäfer, L. V.; Marrink, S. J. Partitioning of Lipids at Domain Boundaries in
33 Model Membranes. *Biophys. J.* **2010**, 99, L91-L93.
34
35 48 Barnoud, J.; Rossi G.; Marrink, S. J.; Monticelli, L. Hydrophobic Compounds
36 Reshape Membrane Domains. *PLoS Comput. Biol.* **2014**, 10, e1003873.
37
38 49 Palmieri, B.; Yamamoto, T.; Brewster, R. C.; Safran, S. A. Line Active Molecules
39 Promote Inhomogeneous Structure in Membranes: Theory, Simulations and
40 Experiments. *Adv. Colloid Interface Sci.* **2014**, 208, 58-65.
41
42 50 Garcia-Sáez, A. J.; Chiantia, S.; Schwille, P. Effect of Line Tension on the
43 Lateral Organization of Lipid Membranes. *J. Biol. Chem.* **2007**, 282, 33537-
44 33544.
45
46
47
48
49
50
51
52
53
54
55
56
57
58
59
60

- 1
2
3 51 Hadduck, A. N.; Hindagolla, V.; Contreras, A. E.; Li, Q.; Bakalinsky, A. T. Does
4 Aqueous Fullerene Inhibit the Growth of *Saccharomyces Cerevisiae* or
5 *Escherichia Coli*? *Appl. Environ. Microbiol.* **2010**, 76, 8239-8242.
6
7
8 52 Kang, S.; Mauter, M. S.; Elimelech, M. Microbial Cytotoxicity of Carbon-Based
9 Nanomaterials: Implications for River Water and Wastewater Effluent.
10 *Environ. Sci. Technol.* **2009**, 43, 2648-2653.
11
12
13 53 Chiron, J. P.; Lamande, J.; Moussa, F.; Trivin, F.; Céolin, R. Effect of
14 "Micronized" C₆₀ Fullerene on the Microbial Growth in Vitro, *Ann. Pharm. Fr.*
15 **2000**, 58, 170-175.
16
17
18 54 An, H.; Jin, B. Fullerenols and Fullerene Alter Cell Growth and Metabolisms of
19 *Escherichia Coli*. *J. Biomed. Nanotechnol.* **2015**, 11, 1261-1268.
20
21
22
23
24
25
26
27
28
29
30
31
32
33
34
35
36
37
38
39
40
41
42
43
44
45
46
47
48
49
50
51
52
53
54
55
56
57
58
59
60

TOC Graphic



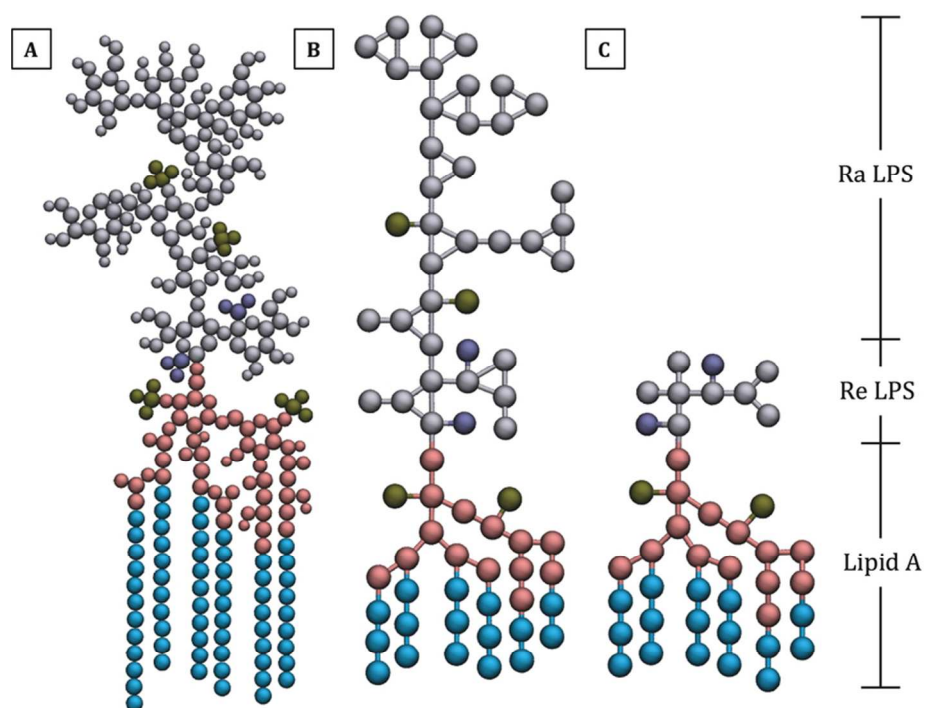


Figure 1: CG mapping schemes for Re and Ra LPS (A) The UA model for Ra LPS is shown alongside the CG model for (B) Ra LPS, and (C) Re LPS. Carbon tails are colored cyan, phosphate groups are colored brown, carboxylate groups are colored dark blue, glucosamine and glycerol groups are colored pink, and the remaining core saccharide sections are colored silver.

Figure 1

81x61mm (300 x 300 DPI)

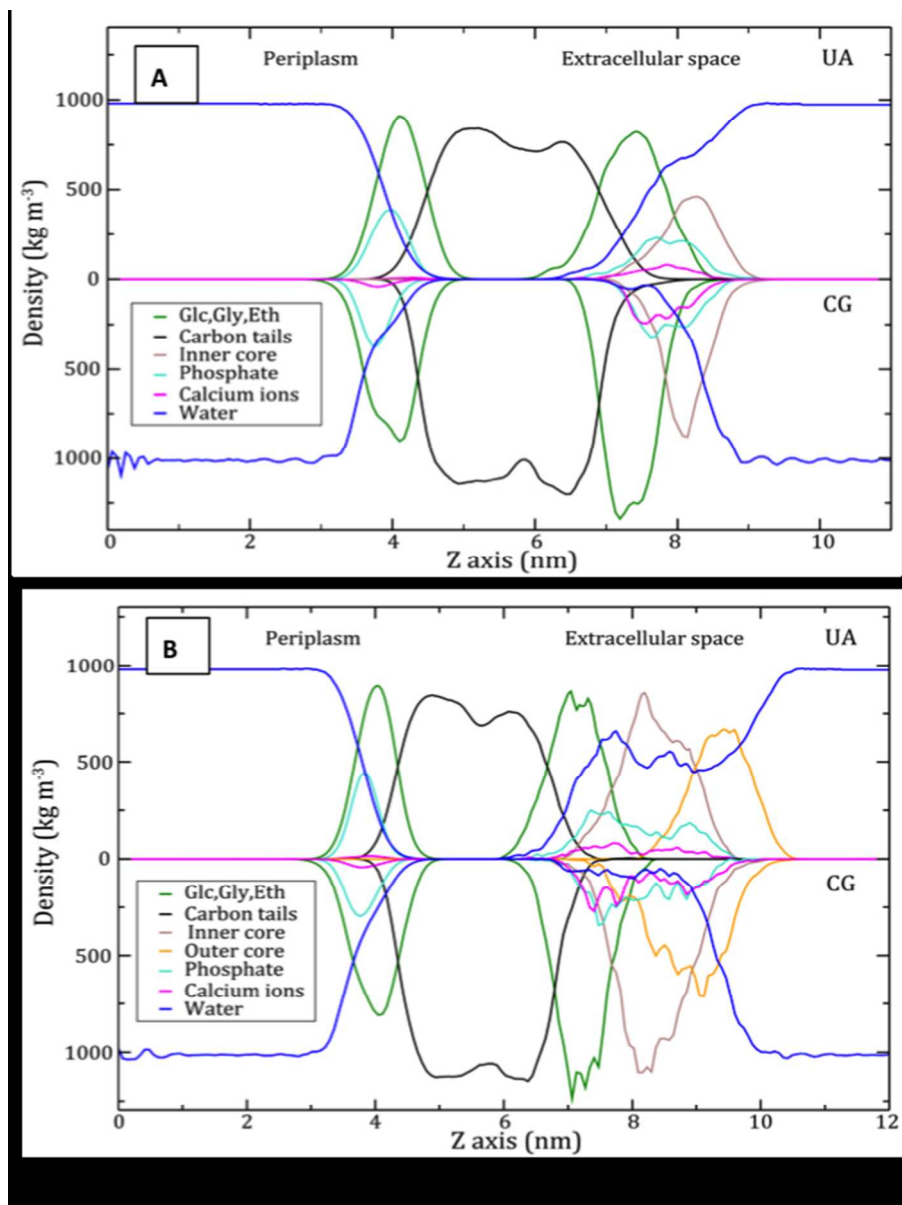


Figure 2: Comparative partial mass density plots for *E. coli* outer membranes. *E. coli* membranes were simulated at 310 K using CG and UA representations. The first membrane was built with a leaflet of (A) Re LPS, while the second membrane contained a leaflet of (B) Ra LPS instead. Carbon tails are represented by black lines, glucosamine, glycerol and ethanolamine groups (Glc,Gly,Eth) are represented by green lines, phosphate groups are represented by turquoise lines, calcium ions are represented by pink lines, inner core sugars are represented by brown lines, outer core sugars are represented by orange lines, and water is represented by blue lines. The partial mass densities are measured along the bilayer normal (Z axis).

Figure 2

114x152mm (150 x 150 DPI)

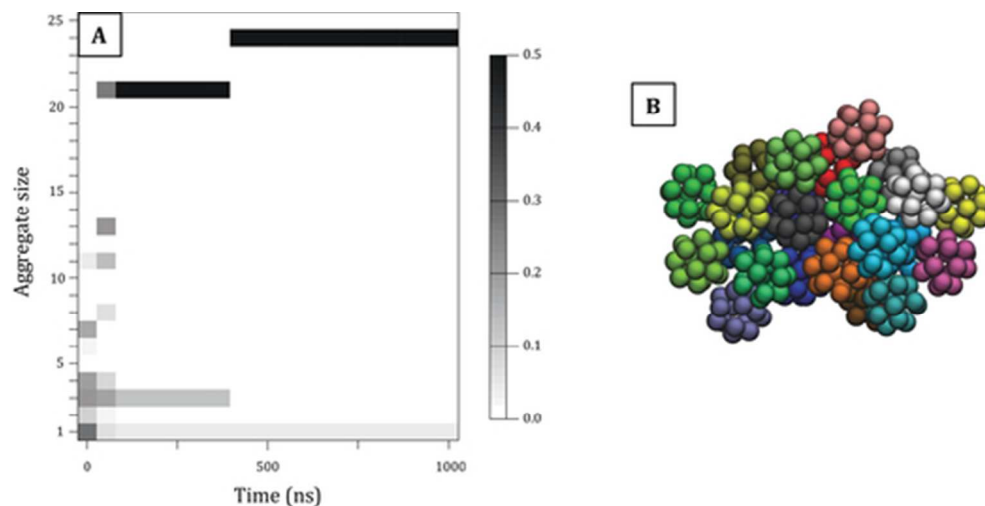


Figure 3: Clustering of C60 in a representative CG simulation (A) The clustering of C60 is plotted as a function of time during the first 1 μ s of a CG simulation. The grayscale in each cell represents the fraction of C60 involved in an aggregate of a given size (y axis) at a given time (x axis). The C60 concentration was 1.13 mM. (B) Snapshot of the 24-unit C60 cluster formed toward the end of this initial period of aggregation.

Figure 3

45x22mm (300 x 300 DPI)

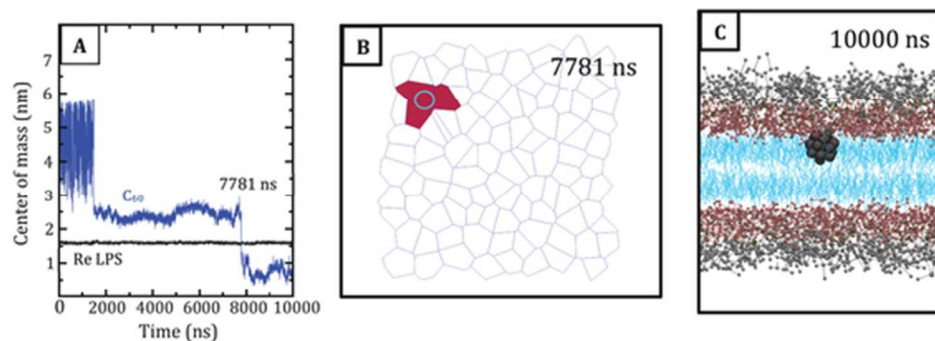


Figure 4: The effect of sodium ions on Re LPS bilayer permeability. (A) Position of the C₆₀ monomer along the bilayer normal, relative to the Re LPS bilayer center. The blue line depicts the center of mass coordinates for the C₆₀ monomer from the bilayer center, while the black line shows the average position of LPS boundary phosphate groups in a single leaflet of the bilayer. The simulation was performed at 310 K, with a single C₆₀ fullerene. (B) Two-dimensional voronoi tessellation of the Re LPS surface as the C₆₀ fullerene bypasses the phosphate barrier at 7781 ns. Each cell represents a single Re LPS head group. The red cells correspond to the LPS head groups adjacent to the C₆₀ monomer. The cyan circle shows the position of the C₆₀ monomer during the head group tunneling event. (C) Side-view snapshot for the C₆₀ monomer after it bypassed the phosphate interface to settle in the lipid core.

Figure 4

51x19mm (300 x 300 DPI)

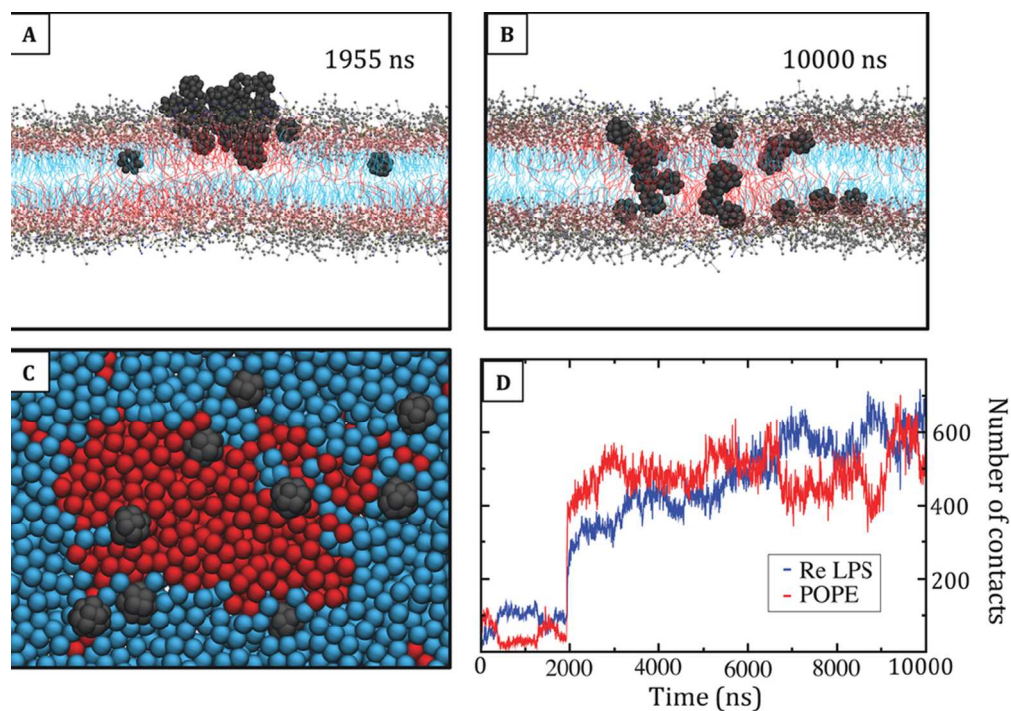


Figure 5: Migration of C60 fullerenes to the POPE-Re LPS lipid interface. (A) The C60 cluster migrates to the domain of POPE, and slips past the hydrophilic head groups to access the lipid core. (B) The cluster disaggregates, and the disbanded fullerenes drift to the interface between the separate POPE and LPS domains. The Re LPS are colored as before, and the POPE lipid tails are colored red. (C) Top-view snapshot of the disbanded fullerenes at the POPE-Re LPS lipid interface. The lipid head groups are omitted for clarity. (D) The number of contacts between the C60 fullerenes and the (Re LPS and POPE) acyl tails is plotted as a function of simulation time. The red line shows the number of contacts between the fullerenes and POPE lipid tails, while the blue shows the number of contacts between the fullerenes and the Re LPS lipid tails. The relative number of contacts was determined using a 0.6 nm cutoff distance.

Figure 5
85x61mm (300 x 300 DPI)

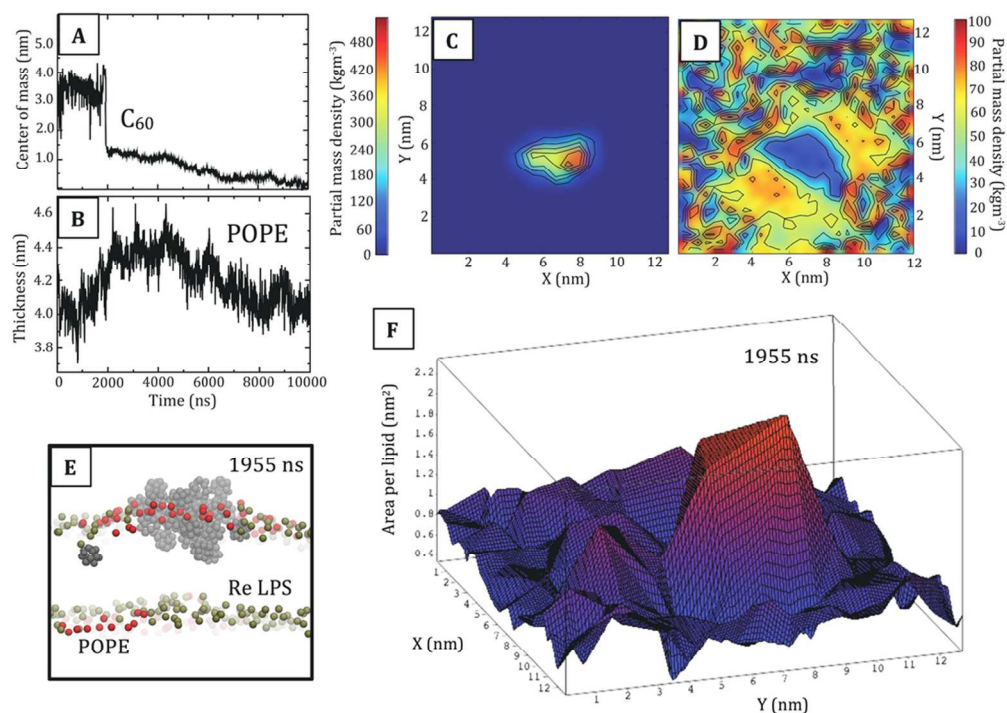
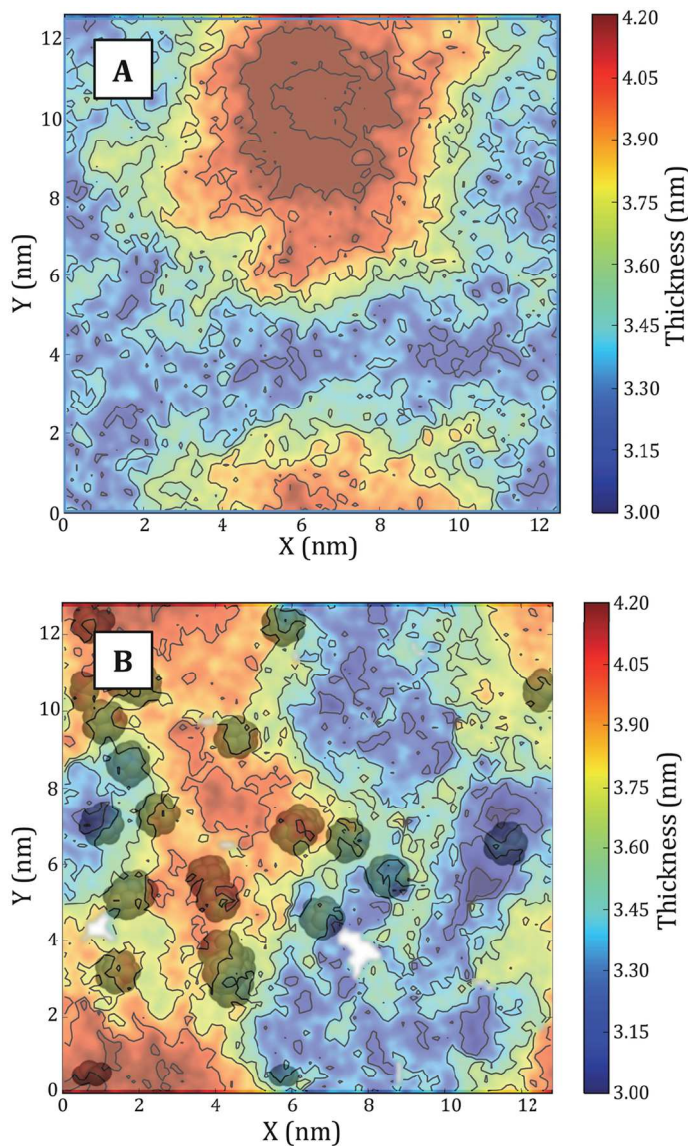


Figure 6: Translocation of a C60 cluster across the water-lipid interface. (A) Average center of mass coordinates for C60 fullerenes along the bilayer normal (relative to the bilayer center). (B) Average thickness of the POPE lipids plotted against simulation time; thickness was defined as the distance between POPE phosphate head groups and the bilayer center. (C) Two-dimensional partial mass density for C60 fullerenes comprising the C60 cluster, during the bilayer insertion event (1955 ns). (D) Partial mass densities for Re LPS phosphate and POPE choline head groups during fullerene cluster insertion (1955 ns). The POPE head groups move apart to create a transient micropore whose shape and projected surface area match those of the C60 cluster. (E) Side-view snapshot of the C60 cluster traversing the phosphate interface, the Re LPS phosphate groups are colored brown, the POPE phosphate groups are colored red. All other membrane components are omitted for clarity. (F) Three-dimensional projection of area per lipid values for the membrane leaflet that the C60 fullerenes pass through. The tessellation of area per lipid was performed for the membrane surface at 1955 ns. Red color represents high area per lipid while blue color represents low area per lipid.

Figure 6

92x70mm (300 x 300 DPI)



C60 fullerenes promote lipid mixing in the multicomponent membrane. After the C60 fullerenes had entered the bilayer core, they migrated to the boundaries between the coexisting POPE and Re LPS domains. The fullerenes then reduced the line tension between the coexisting lipid fractions by minimizing structural mismatch. The figures depict the bilayer thickness as a two-dimensional landscape for the membrane (A) without any C60 fullerenes dissolved in the lipid core, and (B) with 25 C60 fullerenes dispersed among the lipid tails. The final C60 particle positions are depicted above the thickness landscape as translucent black spheres (for reference).

Figure 7

105x170mm (300 x 300 DPI)

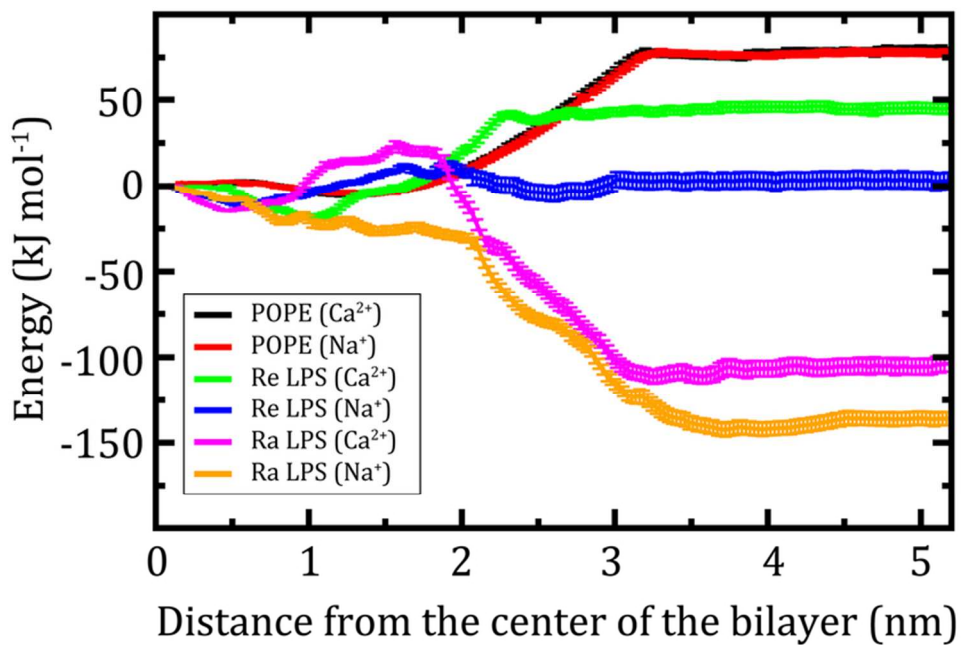


Figure 8: PMF profiles for C60 fullerene as a function of distance from the center of homogeneous lipid bilayers. PMF profiles for C60 fullerene as a function of distance from the bilayer center. The red line shows the data for the POPE bilayer with Na⁺ ions, the black line shows the data for the POPE bilayer with Ca²⁺, the green line shows the data for the Re LPS bilayer with Ca²⁺ ions, the blue line shows the data for the Re LPS bilayer with Na⁺, the pink line shows the data for the Ra LPS bilayer with Ca²⁺ ions, and the orange line shows the data for the Ra LPS bilayer with Na⁺ ions. Each umbrella sampling simulation was 1 μ s long; the simulation temperature was 310 K; the umbrella sampling windows were separated by distances of 0.2 nm. The free energy was set to zero at the bilayer center.

Fig 8

37x29mm (600 x 600 DPI)